Journal of Power Sources 253 (2014) 381–391

Contents lists available at ScienceDirect

Journal of Power Sources

journal homepage: www.elsevier.com/locate/jpowsour

On the estimation of high frequency parameters of Proton Exchange Membrane Fuel Cells via Electrochemical Impedance Spectroscopy

J. Mainka [a,b,*], G. Maranzana [a,b], J. Dillet [a,b], S. Didierjean [a,b], O. Lottin [a,b]

[a] Laboratoire d'Energétique et de Mécanique Théorique et Appliquée (LEMTA), Université de Lorraine, 2, avenue de la Forêt de Haye, 54504 Vandoeuvre-lès-Nancy, France
[b] LEMTA, CNRS, 2, avenue de la Forêt de Haye, 54504 Vandoeuvre-lès-Nancy, France

HIGHLIGHTS

- The estimation of impedance parameters of H_2/air PEMFC with Randles EEC is discussed.
- Sensitivity analysis gives validity domain for estimation of cathode parameters.
- EIS allows clear separation between charge and mass transfer voltage losses.
- Cathode kinetics parameters were estimated from the charge transfer resistance.
- EIS is more precise and fast than steady-state methods for cathode characterization.

ARTICLE INFO

Article history:
Received 16 September 2013
Received in revised form
3 December 2013
Accepted 10 December 2013
Available online 21 December 2013

Keywords:
Polymer electrolyte membrane fuel cell
Electrochemical Impedance Spectroscopy
Parameter estimation
Cathode
Modeling

ABSTRACT

This paper is a discussion on the estimation of impedance parameters of H_2/air fed Proton Exchange Membrane Fuel Cells (PEMFC). The impedance model corresponds to the Randles electrical equivalent circuit accounting for charge separation and transport processes in the cathode catalyst layer, as well as for oxygen diffusion through the backing layer. A sensitivity analysis confirms that the cathode parameters are not correlated and that the consideration of the anode has no significant impact on the estimation of their values. In addition, it is shown that the diffusion parameters have a significant impact in the low frequency domain only, at least with this model. The parameters characterizing charge separation and transport processes at the cathode can thus be estimated with the high frequency impedance data, independently of the oxygen transport model. Consequently, even in the absence of a fully validated oxygen transport impedance, EIS can be used as an alternative method (to classical steady-state methods) for the estimation of the parameters characterizing the cathode reaction: the Tafel slope b, the charge transfer coefficient α and possibly, the exchange current density j_0. This reduces significantly the measuring time while enhancing the accuracy by comparison with steady-state methods.

1. Introduction

Applied to fuel cells, Electrochemical Impedance Spectroscopy (EIS) is a powerful diagnosis tool that can be used during operation with minimal perturbations [1–3]. For a comprehensive review about the application of EIS to Proton Exchange Membrane Fuel Cells (PEMFC) we refer to the works of Yuan et al. [4] and Niya and Hoorfar [5] giving an overview of recent advances in this field.

EIS allows to analyze in the frequency domain the different physical and chemical processes occurring in a fuel cell by imposing small harmonic perturbations to the system and measuring the impedance. Consequently, this technique can be used for in-situ and ex-situ studies which makes it a polyvalent and accurate tool by comparison with most of the classical electrochemical (steady-state) methods. A common application of EIS is the identification of the origin of the different potential losses (*i.e.*, ohmic, kinetic and mass transport losses) and their estimation [1,2,6–9] with the focus to optimize the MEA design [10] and to determine optimal working conditions [1,11]. Beside this, it is possible to determine the electrical properties of the fuel cell components, materials and interfaces [12], as well as their dependence on the operating

* Corresponding author. LEMTA, CNRS, 2, avenue de la Forêt de Haye, 54504 Vandoeuvre-lès-Nancy, France.
E-mail address: julia.mainka@univ-lorraine.fr (J. Mainka).

0378-7753/$ – see front matter © 2013 Elsevier B.V. All rights reserved.
http://dx.doi.org/10.1016/j.jpowsour.2013.12.064

conditions [2,13,14] and on aging effects like carbon corrosion at the cathode [15], catalyst poisoning by carbon monoxide [14,16] at the anode or corrosion of the flow field plates [17]. EIS can also be used for the estimation of the catalytic active area [9], although other electrochemical techniques (*e.g.*, cyclic voltammetry) are more appropriate. The water management and the MEA humidification playing an important role in the electrical efficiency of a fuel cell, numerous EIS studies focus on the detection of dry and flooded conditions and on their influence on the fuel cell operation [1,9,14].

Obtaining reliable information about the physical processes that occur in a fuel cell is not a simple task since they are strongly coupled. The experimental impedance spectra are usually interpreted in terms of equivalent electrical circuits (EEC) consisting of an assembly of resistances R, capacitances C and inductances L. Almost all experimental impedance spectra in the right side of the complex plane can be fitted with an EEC provided that it contains enough R/C elements in parallel. As a consequence, a multitude of more or less sophisticated EECs can be found in the literature to describe all possible forms of impedance spectra. However, in order to identify the origin(s) of voltage drop(s), the elements of the electrical circuit have to be consistent with the physical phenomena occurring in the cell. In addition, for their simultaneous independent estimation, the impedance parameters have to be decorrelated. Hence, this paper does not aim to present a new impedance model, but to discuss about the validity of the estimation of the parameters that characterize charge separation and transfer processes in H_2/air fed PEMFC when using EIS: the discussion is based on numerical and experimental studies using the simple and commonly used Randles EEC [18].

In this circuit, charge separation and transport are accounted for by a high frequency resistance, a charge transfer resistance, and a double-layer capacity. The oxygen transport through the porous media at the cathode is modeled by a finite Warburg element [19], which results from simple assumptions: one-dimensional transport by diffusion only, surface reaction and a constant O_2 concentration at the GDL/air channel interface. Since the oxygen transport parameters depend strongly on the chosen impedance model [20–22], we focus on the estimation of those characterizing the ORR. It is shown that their values can be estimated independently of the oxygen transport impedance through the analysis of the impedance spectra in the high frequency domain only. Some results of the estimation of parameters characterizing the cathode reaction are presented, *i.e.*, the Tafel slope b and the charge transfer coefficient α (or the exchange current density j_0) vs. the current density. Usually, these parameters are determined using steady-state methods (*e.g.*, the Tafel plot), which leads to two (or three) averaged values being associated with the low (the intermediate) and the high current density regimes [23–26]. Former studies show that EIS can be used as an alternative to the polarization curve for the determination of the Tafel slope [24,25]. However, in these studies, the values of b are averaged over the low and high frequency ranges. In contrast, we show that EIS can be used to estimate not only b, but also α, and possibly j_0 at a given operating point with one single impedance measurement. In addition, their estimation using the impedance data at high frequencies only is independent of oxygen transport losses, which characteristic timescales correspond to much lower frequencies. This separation of ORR parameters from oxygen transport is not always possible when using steady-state methods. EIS could thus not only reduce the measuring time, but also enhance the precision of the estimation of the reaction parameters of the cathode.

In the second part of this work, we present results of a sensitivity analysis ensuring the absence of correlation between the model parameters, which is a necessary condition for their reliable estimation. More generally, the sensitivity analysis allows to point out the abilities and limits of the impedance model in the considered operating conditions. The anode is usually neglected in impedance analyses because the voltage drops caused by this electrode are significantly smaller than those originating from the cathode [8,9,13,27,28]. This hypothesis is also tested through the sensitivity analysis.

2. Theory

The expression of the cell impedance that is used for the parameters estimation is derived in the following. In section 2.1, the expressions of the cell potential and current are presented. These expressions are used in Section 2.2 for the derivation of the cell impedance.

Fig. 1 shows a schematic representation of the MEA geometry. The structure is assumed symmetric to the membrane. The main hypotheses of the model are:

- The fuel cell is isothermal and isobaric.
- The description of the transport phenomena is one-dimensional, the x-axis being oriented from the anode to the cathode.
- The diffusion media at the anode and the cathode are homogeneous.
- The catalyst layers are considered as additional diffusion media of a thickness of about 10 μm. Consequently, we assume a surface reaction (at $x = 0$) and a constant oxygen concentration at the GDL/air channel interface (at $x = \delta$).
- The cell being fed with pure hydrogen, the diffusion limitations are negligible at the anode side and $c_{H_2}(x = 0) = c^*_{H_2}$.
- Oxygen transport is assumed to occur by Fickian diffusion only.

The anode is taken into account in order to estimate its influence on the identification of the cathode impedance parameters.

Note that the assumption of one-dimensional mass transport is valid for small area MEAs only. In a more general case, two dimensional mass transport phenomena like oxygen depletion [20] and concentration oscillations induced by the measuring signal propagating along the cathode gas channel [29–31] have to be taken into account.

2.1. System equations

In a general way, the cell voltage can be expressed by

$$E_{\mathrm{cell}}(t) = E_0 - R_{\mathrm{hf}} \times j_{\mathrm{cell}}(t) - \eta_{\mathrm{c}}(t) - \eta_{\mathrm{a}}(t), \tag{1}$$

where E_0 denotes the open circuit voltage (OCV) and R_{hf} an ohmic resistance accounting for the ionic resistance of the membrane as well as for the electronic resistances of the various MEA components (catalyst layer, GDL, flow field plates). η_{c} and η_{a} stand for the voltage losses resulting from the finite rate of the cathode and anode reactions, respectively.

With reference to the catalyst area, the values of the exchange current density at the cathode $j_{0,\mathrm{c}}$ are commonly comprised between 10^{-6} A $\mathrm{cm}^{-2}_{\mathrm{Pt}}$ and 10^{-9} A $\mathrm{cm}^{-2}_{\mathrm{Pt}}$ [9,23,24,32]. Assuming an electrode roughness $\gamma = 100$, the values of $j_{0,\mathrm{c}}$ vary between 10^{-4} A $\mathrm{cm}^{-2}_{\mathrm{macro}}$ and 10^{-7} A $\mathrm{cm}^{-2}_{\mathrm{macro}}$ with reference to the macroscopic area of the MEA ($A_{\mathrm{macro}} = A_{\mathrm{Pt}}/\gamma$), which is significantly lower than the current densities of an operating cell. In addition, the O_2 diffusivity through the pores of the GDL and catalyst layer is limited, especially when the cell is fed with air instead of pure O_2 [28]. This phenomenon is reinforced by a possible flooding of the gas pores in the presence of liquid water. The oxygen concentration is consequently lower at the electrode $c_{O_2}(x = 0, t)$ than at the GDL/air channel interface $c_{O_2}(x = \delta, t) = c^*_{O_2}$. The oxygen reduction reaction (ORR) is thus irreversible and η_{c} can be described by a Tafel law of the form

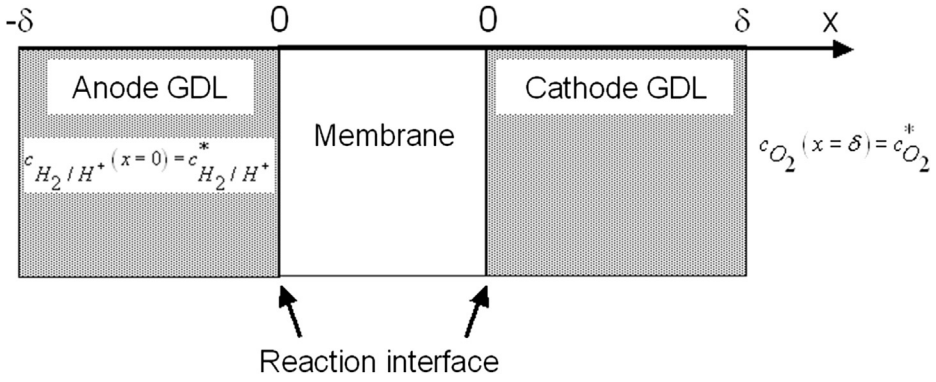

Fig. 1. Schematic representation of the MEA geometry.

$$\eta_c(t) = b_c \ln\left[\frac{j_{f,c}(t)\times c^*_{O_2}}{j_{0,c}\times c_{O_2}(x=0,t)}\right] \tag{2}$$

The exchange current density at the anode $j_{0,a}$ varies generally between 5×10^{-4} A cm^{-2}_{Pt} and 3×10^{-2} A cm^{-2}_{Pt} in acidic media [24,33–35]. This results in a macroscopic exchange current density comprised between 0.05 A cm^{-2}_{macro} and 3 A cm^{-2}_{macro} ($\gamma = 100$), which is in the range of the output current densities. The hydrogen oxidation reaction (HOR) can therefore be considered as reversible and it must consequently be described by the Butler–Volmer equation

$$\begin{aligned} j_{f,a}(t) =& j_{0,a}\left[\frac{c_{H_2}(x=0,t)}{c^*_{H_2}}\exp\left(\frac{\eta_a(t)}{b_{a,H_2}}\right)\right. \\ &\left. -\frac{c_{H^+}(x=0,t)}{c^*_{H^+}}\exp\left(-\frac{\eta_a(t)}{b_{a,H^+}}\right)\right] \end{aligned} \tag{3}$$

To simplify the notations, it is supposed that the proton transport is significantly faster than the reaction rate, which implies that $c_{H^+}(x=0,t) = c^*_{H^+}$. When working with pure hydrogen, mass transport is not limiting [36] and we consider that the H_2 concentration at the electrode is equal to that in the channel $c^*_{H_2}$. Finally, we assume equal values for the Tafel slope of the two half reactions at the anode ($b_{a,H_2} = b_{a,H^+} = b_a$ [24]), and (3) simplifies to

$$j_{f,a}(t) = j_{0,a}\left[\exp\left(\frac{\eta_a(t)}{b_a}\right) - \exp\left(-\frac{\eta_a(t)}{b_a}\right)\right]. \tag{4}$$

The parameters $b_{c,a}$ in Eqs. (2) and (4) denote the Tafel slopes for the two half reactions at the cathode and anode respectively which are defined as

$$b_{c,a} = \frac{RT}{\alpha_{c,a}nF}, \tag{5}$$

where $\alpha_{c,a}$, are the respective charge transfer coefficients and n the number of exchanged electrons. By convention, the overpotential and the current density are usually counted negative at the cathode and positive at the anode. However, for the sake of simplicity, we consider only positive values of η_m, $j_{f,m}$ and $j_{0,m}$ at both electrodes ($m = a,c$).

The cell current density $j_{cell}(t)$ is the sum of the faradaic $j_f(t)$ and the capacitive current density $j_c(t) = C_{dl,m}\times\partial\eta_m/\partial t$

$$j_{cell}(t) = j_{f,m}(t) + C_{dl,m}\frac{\partial\eta_m}{\partial t}, \tag{6}$$

where $C_{dl,m}$ stands for the double-layer capacity at electrode m. In steady-state, the capacitive contribution to the current is zero, which implies that $\langle j_{f,c}\rangle_t = \langle j_{f,a}\rangle_t = \langle j_{cell}\rangle_t$. Note that the current densities refer to the macroscopic area of the MEA.

2.2. Cell impedance

In the dynamic regime, the cell impedance is defined by the ratio of the variation of the cell potential to that of the cell current density and reads as

$$Z_{cell} = \frac{\Delta\bar{E}_{cell}}{-\Delta\bar{j}_{cell}}. \tag{7}$$

In order to derive an explicit expression of Z_{cell}, the variables have to be decomposed in their steady-state and dynamic components. Assuming harmonic oscillations of small amplitude, each variable X ($X = E_{cell}, j_{cell}, j_{f,m}, \eta_m, c_{O_2}$) can be decomposed into its steady-state value $\langle X\rangle_t$ and a sinusoidal component of amplitude $\Delta\bar{X}$, leading to

$$\begin{aligned} E_{cell}(t) &= \langle E_{cell}\rangle_t + \Delta\bar{E}_{cell}\exp(i\omega t) \\ j_{cell}(t) &= \langle j_{cell}\rangle_t + \Delta\bar{j}_{cell}\exp(i\omega t) \\ j_{f,m}(t) &= \langle j_{cell}\rangle_t + \Delta\bar{j}_{f,m}\exp(i\omega t) \\ \eta_m(t) &= \langle\eta_m\rangle_t + \Delta\bar{\eta}_m\exp(i\omega t) \\ c_{O_2}(x,t) &= \langle c_{O_2}(x)\rangle_t + \Delta\bar{c}_{O_2}(x)\exp(i\omega t). \end{aligned} \tag{8}$$

The overbars denote complex numbers. The amplitudes of the system parameters can be derived from (1)–(6) which results in

$$\begin{aligned} \Delta\bar{E}_{cell} &= -R_{hf}\times\Delta\bar{j}_{cell} - \Delta\bar{\eta}_c - \Delta\bar{\eta}_a \\ \Delta\bar{\eta}_c &= b_c\frac{\Delta\bar{j}_{f,c}}{\langle j_{cell}\rangle_t} - b_c\frac{\Delta\bar{c}_{O_2}(0)}{\langle c_{O_2}(0)\rangle_t} \\ \Delta\bar{j}_{f,a} &= \frac{j_{0,a}}{b_a}\left[\exp\left(\frac{\langle\eta_a\rangle_t}{b_a}\right) + \exp\left(-\frac{\langle\eta_a\rangle_t}{b_a}\right)\right]\Delta\bar{\eta}_a \\ \Delta\bar{j}_{cell} &= \Delta\bar{j}_{f,m} + i\omega C_{dl,m}\times\Delta\bar{\eta}_m. \end{aligned} \tag{9}$$

Using (9) in (7) allows to write the cell impedance in an explicit form

$$\begin{aligned} Z_{cell} = R_{hf} &+ \left(\frac{1}{\frac{b_c}{\langle j_{cell}\rangle_t} - \frac{b_c}{\langle c_{O_2}(0)\rangle_t}\frac{\Delta\bar{c}_{O_2}(0)}{\Delta\bar{j}_{f,c}}} + i\omega C_{dl,c}\right)^{-1} \\ &+ \left(\frac{j_{0,a}}{b_a}\left[\exp\left(\frac{\langle\eta_a\rangle_t}{b_a}\right) + \exp\left(-\frac{\langle\eta_a\rangle_t}{b_a}\right)\right] + i\omega C_{dl,a}\right)^{-1}. \end{aligned} \tag{10}$$

To simplify the notations, we introduce:

- The anode charge transfer resistance

$$R_{ct,a} = \frac{\partial \eta_a}{\partial j_{f,a}} = \frac{\Delta \overline{\eta}_a}{\Delta \bar{j}_{f,a}} = \frac{b_a}{j_{0,a}}\left[\exp\left(\frac{\langle \eta_a \rangle_t}{b_a}\right) + \exp\left(-\frac{\langle \eta_a \rangle_t}{b_a}\right)\right]^{-1}. \tag{11}$$

- The cathode charge transfer resistance

$$R_{ct,c} = \frac{\partial \eta_c}{\partial j_{f,c}} = \frac{b_c}{\langle j_{cell} \rangle_t}. \tag{12}$$

- The oxygen transport impedance

$$Z_{c_{O_2}} = -\frac{b_c}{\langle c_{O_2}(0) \rangle_t} \frac{\Delta \overline{c}_{O_2}(0)}{\Delta \bar{j}_f}. \tag{13}$$

An appropriate oxygen transport model is required to obtain an explicit expression of Z_{cO2}, because the estimation of the oxygen diffusion parameters (D^{eff},δ) depends strongly on the transport phenomena taken into account by the model. A detailed study about oxygen transport impedance expressions would be beyond the scope of this work. For more information, see for example [20–22,29,30]. In the present study, oxygen transport is accounted for by a finite Warburg impedance Z_W allowing a first rough estimation of D^{eff} and δ [37]. The Warburg impedance (14) is obtained by solving the Fick diffusion equations in the dynamic regime with the boundary conditions depicted in Fig. 1 [19]. This corresponds to a purely diffusive one-directional oxygen transport through homogeneous porous media and Z_W is given by

$$Z_W = R_d \frac{\tanh\sqrt{i\omega\tau_d}}{\sqrt{i\omega\tau_d}}, \tag{14}$$

where the diffusion resistance R_d corresponds to the low frequency limit of Z_W

$$R_d = \lim_{\omega \to 0} = \frac{b_c \delta}{4FD^{eff}\langle c_{O_2}(0) \rangle_t}, \tag{15}$$

and τ_d is the characteristic diffusion time

$$\tau_d = \frac{\delta^2}{D^{eff}}. \tag{16}$$

The time-averaged oxygen concentration at the reaction interface $\langle c_{O_2}(0) \rangle_t$ is obtained by solving the Fick equation in steady-state, leading to [20]

$$\langle c_{O_2}(0) \rangle_t = c^*_{O_2} - \frac{\langle j_{cell} \rangle_t \delta}{4FD^{eff}}. \tag{17}$$

It is worth mentioning that R_d and τ_d depend both on the diffusion thickness δ and effective oxygen diffusion coefficient D^{eff}. The Warburg impedance can thus also be expressed as a function of these variables: $Z_W(\delta, D^{eff})$. The effective diffusivity accounts for the geometrical properties of the medium through the porosity ε and the tortuosity τ and for the presence of liquid water which impacts their values. D^{eff} is usually expressed in the form of Archie's law [38,39].

With these assumptions, the cell impedance Z_{cell} (10) can be written as

$$Z_E = R_{hf} + \left(\frac{1}{R_{ct,c} + Z_W} + i\omega C_{dl,c}\right)^{-1} + \left(\frac{1}{R_{ct,a}} + i\omega C_{dl,a}\right)^{-1}. \tag{18}$$

Fig. 2 represents the cell impedance described by Eq. (18) in terms of equivalent electrical circuits. The anode EEC is composed by a charge transfer resistance $R_{ct,a}$ in parallel with a double-layer capacity $C_{dl,a}$ (dashed lines). The membrane and the cathode are represented by Randles EEC [18] including a high frequency resistance R_{hf}, a charge transfer resistance $R_{ct,c}$, a double-layer capacity $C_{dl,c}$ and a finite Warburg impedance Z_W [19] (solid lines).

3. Experimental setup

The experimental results are obtained with the mono-channel single cell presented in Fig. 3. The serpentine flow fields (of 0.7×1.0 mm^2 in section and 33 cm in length) are symmetric at the anode and cathode. Although only global impedance data are treated in this work, it must be noted that the cell was designed to perform also locally resolved EIS [37].

The MEA (Johnson Matthey) with a flat area $A_{macro} = 7.87$ cm^2 consists of a PFSA (Gore) polymer membrane of thickness $\delta_m = 30$ μm and active layers ($\delta_{al} \approx 10$ μm) with an average Pt loading of 0.4 mg$_{Pt}$ cm^{-2}. The GDL (Toray™ TGP-H-060) is 190 μm thick with a porosity (without compression) $\varepsilon = 0.78$. The fuel cell is fed in counter-flow (at 1 atm) with dry hydrogen and humidified air with the corresponding stoichiometry factors: $S_{H_2} = 1.2$ and $S_{air} = 3$. The air is humidified ($RH \approx 78\%$) and pre-heated thanks to a bubbler. The connecting pipes are slightly heated in order to avoid condensation between the outlet of the bubbler and the air channel inlet. The cell temperature is controlled ($T_{cell} = 56 \pm 1$°C) by an electric heating system fixed to the anode bipolar plate. Thermal gradients exist probably within the cell because of the thermal resistances of the various components and those of the interfaces between them [40].

The impedance measurements are performed in galvanostatic mode at frequencies ranging logarithmically from 0.025 Hz to 500 Hz with a resolution of 10 points per decade. The peak-to-peak sinusoidal perturbation is comprised between 5% and 10% of the cell current (at $\langle j_{cell} \rangle_t = 0.5$ A cm^{-2}, 25 mA cm^{-2} $\leq \Delta \bar{j}_{cell} \leq$ 50 mA cm^{-2} and 31 mV $\leq \Delta \bar{E}_{cell} \leq$ 62 mV). It was checked that in this range, the AC signal amplitude does not affect the impedance measurements.

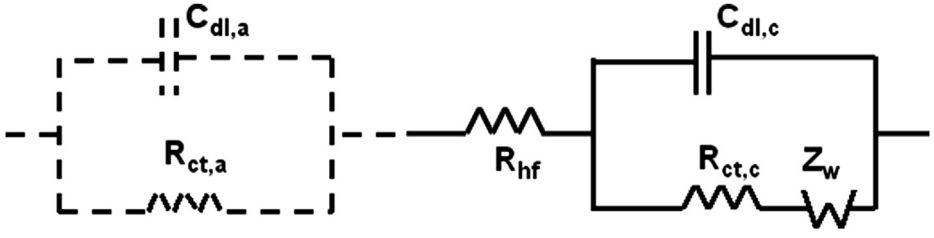

Fig. 2. MEA equivalent electrical circuit(s). Dashed lines: anode equivalent circuit used for sensitivity analysis only. Solid lines: Randles equivalent circuit [18] of the cathode and electrolyte used for parameters estimation.

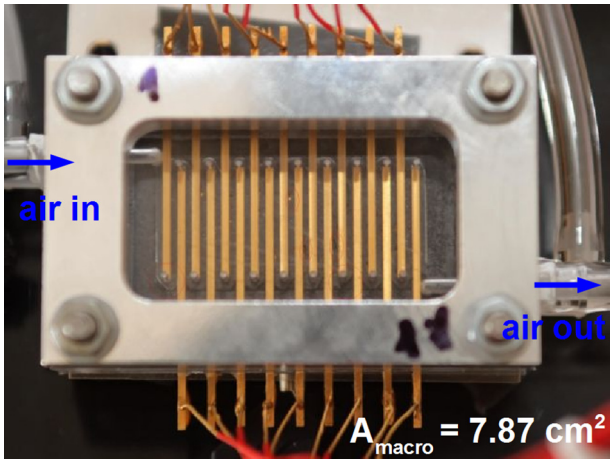

Fig. 3. Mono-channel single cell with a flat area A_{macro} = 7.87 cm^2. The current collectors form the serpentine flow field.

The data acquisition and processing system is depicted in Fig. 4. Since the cell impedance is almost entirely determined by the cathode, the membrane and some contact resistances, it is possible to use the anode as a reference electrode [9]. A passive electronic circuit is used to measure the current intensities with the least possible perturbations: each of the current collectors is connected to a 10 mΩ shunt resistance. The whole experimental setup is controlled by a *Labview* program.

The impedance parameters are determined by fitting the experimental spectra with Eq. (18) using a complex nonlinear least square method. In practice, we use the Matlab function *fminsearch* that determines the minimum of the function ΔZ, defined as the square of the difference between the experimental Z_{exp} and the theoretical impedance Z_{cell} (18) $-\ \Delta Z = (Z_{exp} - Z_{cell})^2$, starting from an initial set of model parameters (R_{hf}, $R_{ct,c}$, $C_{dl,c}$, R_d, τ, $R_{ct,a}$, $C_{dl,a}$). *fminsearch* uses the Nelder–Mead simplex algorithm of Lagarias et al. [41].

4. Results and discussion

In Section 4.1, we present and discuss some results of the parameters estimation characterizing the charge separation and transfer processes at the cathode obtained using the impedance model of the Randles ECC, *i.e.*, the Tafel slope b, the charge transfer coefficient α and the exchange current density j_0. These parameters can be determined with the charge transfer resistance R_{ct} independently of the oxygen transport model by fitting the spectra in the high frequency domain only (cf. sensitivity analysis in Section 4.2). It is worth mentioning that the values of b obtained with R_{ct} depend on the reaction kinetics and on the proton conduction through the electrode volume (*lumped b*). As the cathode parameters only are considered, the subscripts relative to the electrodes (a or c) are omitted in this part to simplify the notations.

A complementary sensitivity analysis relative to the parameters of the impedance expression in Eq. (18) is carried out in Section 4.2 in order to investigate the domain of the validity of the Randles EEC (Fig. 2) used for the estimation of the cathode parameters.

4.1. Estimation of cathode reaction parameters

The following experimental data correspond to mean values resulting from a series of five measurements carried out under identical conditions. The corresponding standard deviations are also shown in the figures. The cell was operated as described in section 3, at current densities j_{cell} comprised between 0.013 A cm^{-2} and 1.1 A cm^{-2}.

Fig. 5 depicts the charge transfer resistance R_{ct} as a function of j_{cell}. The small error bars indicate the good reproducibility of the estimation using the Randles EEC. The uncertainties increase at low current densities. This is related to the higher amplitude of the AC signal (with reference to the DC signal) required to perform the impedance measurements at low current densities.

R_{ct} remains uniform over the major part of the current density range. However, it increases steeply at low current densities ($j_{cell} \leq 0.1$ A cm^{-2}), which is consistent with the steep increase of the activation overpotential in this range. At very low current densities (near the OCV), the ORR can be described by a linearized form of the Butler–Volmer law which results in combination with the definition of R_{ct} at the cathode (12) in

$$R_{ct} = \frac{RT}{2Fj_0}. \tag{19}$$

A more detailed derivation of the above expression is given in the Appendix. It must be noted that R_{ct} is related to the global ORR per mole of produced water ($1/2O_2+2H^+ +2e^- \rightarrow H_20$) so that n is set to 2 in our case. Nevertheless, the expressions of the Tafel slope and of the charge transfer resistance derived above remain valid no matter the number of exchanged electrons.

The values of j_0 are generally comprised between 10^{-4} A cm^{-2} and 10^{-7} A cm^{-2} [9,23,24,32] with reference to the MEA flat surface (with $\gamma = 100$). Starting from these results, the value of the charge transfer resistance near the OCV could be (19):

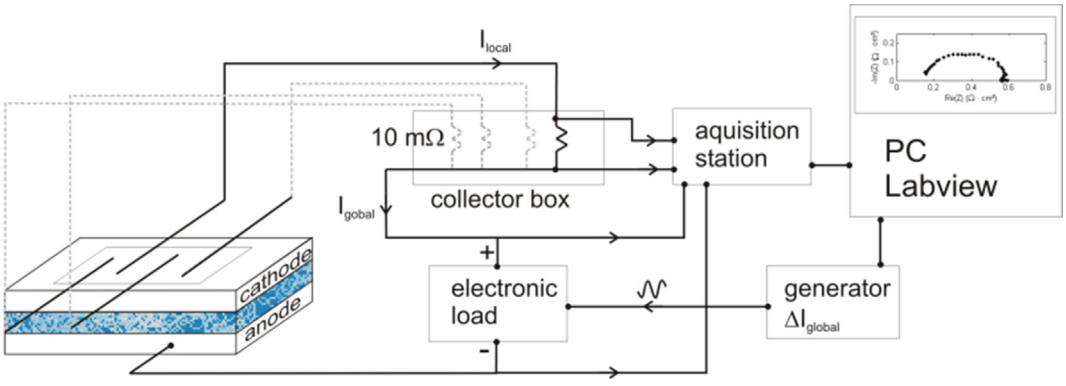

Fig. 4. Data acquisition and processing setup for the impedance measurements.

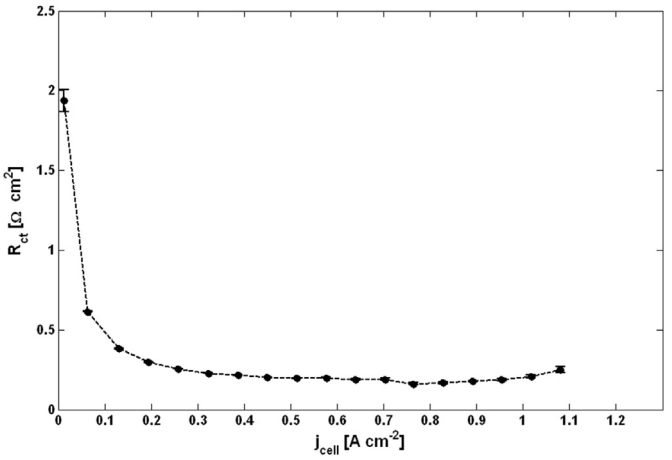

Fig. 5. Cathode charge transfer resistance R_{ct} identified from EI spectra using the Randles equivalent circuit vs. cell current density j_{cell}.

$$j_0 = 10^{-4}\ \text{A cm}^{-2} \rightarrow R_{ct}(OCV) = 71\ \Omega\ \text{cm}^2$$
$$j_0 = 10^{-7}\ \text{A cm}^{-2} \rightarrow R_{ct}(OCV) = 7.1\ 10^4\ \Omega\ \text{cm}^2.$$

The behavior of R_{ct} obtained with our EIS measurements at low current densities is thus consistent with the expectations, notwithstanding the significant variations of the data available in the literature. However, the estimation of the electrode reaction parameters (b and α_c) must be made at current densities where a Tafel law (2) can be used. Consequently, the values of R_{ct} estimated at the lowest experimental current densities ($j_{cell} \leq 0.013$ A cm^{-2}) are not considered in the following.

The most commonly used method for the estimation of the Tafel slope is the Tafel plot (plot of the cathode overpotential vs. the common logarithm of the current density) yielding a straight line of slope b_{10} (expressed in V dec^{-1}) and a y-intercept at $-b_{10}\log(j_0 c_{O_2}/c^*_{O_2})$. This method leads to two (or sometimes three) average values of b_{10}[1] for the oxygen reduction reaction (in Pt/C electrodes): at low current densities ($E > 0.8$ V), $b_{10} \approx 60$ mV dec^{-1} and at high current densities ($E < 0.8$ V), $b_{10} \approx 120$ mV dec^{-1} [8,23,25,42–44]. The change in the Tafel slope is generally explained by a shift in the mechanism from a reduction on a Pt-oxide covered surface (at low current densities) to a reaction on an oxide free surface (at high current densities) characterized by different adsorption isotherms (Langmuir, Temkin) [25,44]. It should be noted that these values are only orders of magnitude and the results reported in the literature vary usually in a range of about 20 mV dec^{-1} depending on temperature, gas pressure, oxidant gas (pure O_2 or air) and investigated system, *i.e.*, single electrode, single cell or stack [9,23–25,42,43]. For instance, by fitting the Tafel plots of a PEMFC operated at 25 °C with H_2 and air at $P = 1$ atm, Ciureanu et al. [9] measured a Tafel slope varying from about 130 mV dec^{-1} to 270 mV dec^{-1}. Regardless of the exact values of b_{10}, all studies in the literature report consistently an increase (doubling) of the Tafel slope from the low to the high current density regime.

Using EIS, the Tafel slope (relative to the MEA macroscopic area) can be determined directly along with the charge transfer resistance: $b = R_{ct} \times j_{cell}$ (12). This presents the advantage of identifying the Tafel slope at a given operating point by one single EI measurement.

Fig. 6 depicts the Tafel slope (in mV dec^{-1}) derived from the charge transfer resistance (Fig. 5) as a function of j_{cell}. b_{10} increases continuously from 23 mV dec^{-1} at $j_{cell} = 0.063$ A cm^{-2} to 384 mV dec^{-1} at $j_{cell} = 1.08$ A cm^{-2}. The resulting values, as well as the increase with the current density are in good agreement with former studies [8,23,25,42–44]. However, instead of the two slopes regime that is usually reported, b_{10} increases continuously. For comparison, we also determined the value of b_{10} from the Tafel plot and obtained $b_{10} = 67$ mV dec^{-1}. This leads to the conclusion that the Tafel plot yields a mean value of b_{10} averaged over the experimental current density range.

The Tafel slope can related to the (cathode) charge transfer coefficient α_c using Eq. (5). Considering the global ORR reaction where $n = 2$ this yields $b = RT/(\alpha_c \times 2F)$. The charge transfer coefficient is an important parameter characterizing the electrochemical activity of an electrode. The usual method consists in estimating this parameter from the polarization curve. The results reported in the literature (cf. Table 1) show a large dispersion of the values [25,26,45,46], all the more so since α_c depends on the temperature in the high slope regime [25].

In the majority of the cases, this parameter is comprised between 1 and 0.4 and decreases with the current density. For modeling purpose, α_c is often set to 0.5, which corresponds to symmetrical forward and backward reactions at the cathode. However, its actual value depends strongly on the operating conditions. Measurements performed by Parthasarathy et al. [25] show a decrease of α_c from 1 (low Tafel slope regime) to 0.5 (high Tafel slope regime). Danilov et al. [26] identify 3 different values of the charge transfer coefficient for low, intermediate and high current densities: their results confirm the decrease of α_c with increasing current density.

Fig. 7 depicts the values of α_c deduced from the charge transfer resistance in Fig. 5 as functions of the current density j_{cell}. The uncertainty on the estimation of α_c increases at low current densities, because of the lower accuracy of the impedance measurements. However, regardless of the lower precision, α_c approaches 1 at low current densities and decreases with increasing cell current. The charge transfer coefficients determined with R_{ct} as well as their variation with the current density are in good agreement with those observed in former studies (cf. Table 1) confirming that EIS can be used as an alternative to Tafel plot. Actually, EIS could possibly provide more precise estimates than the steady-state methods, because α_c can be determined directly for a given operating point.

As mentioned above, the different forms of oxygen adsorption corresponding to different adsorption isotherms influence the

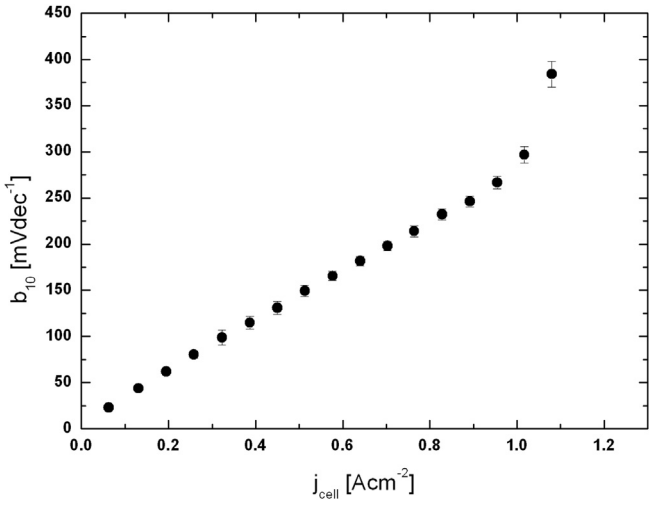

Fig. 6. Tafel slope b_{10} derived from the charge transfer resistance in Fig. 5 vs. j_{cell}.

[1] With $b_{10} = \ln 10 \times b = 2.3 \times b$.

Table 1
Cathode charge transfer coefficient α_c as given in the literature.

T [°C]	Slope regime	α_c	Ref.
70	Low slope	0.95	[25]
	High slope	0.60	
70	Low slope	0.89	[26]
	High slope	0.43	
80	Low slope	1	[32]
	High slope	0.61	

reaction mechanism [25,44] which is lumped in the Tafel slope. For a more precise estimation of α_c the change in the reaction mechanism should be taken into account through the value of n according to the predominant reaction mechanism. Furthermore, note that the charge transfer resistance and the diffusion impedance are correlated at intermediate frequencies, which is shown by the sensitivity analysis presented in the following section. This correlation can also be put forward using oxygen transport models alternative to the classical Warburg approach: the values of R_{ct} (and thus of b_{10} and α_c) change slightly when the parameters estimation is performed with more sophisticated one- and pseudo two-dimensional oxygen transport impedances (accounting for convective effects along and perpendicular to the electrode, as well as for a finite air stoichiometry [20–22]). However, this does not affect the behavior of the electrode reaction parameters as a function of the current density and the results presented above remain qualitatively valid.

4.2. Sensitivity analysis

The following sensitivity analysis aims to verify the reliability of the ECC of Fig. 2 for the estimation of the cathode impedance parameters. To this end, the following issues are considered:

- Possible correlations between the model parameters.
- Possibility to estimate the cathode parameters without modeling the anode.
- Impact of the low frequency parameters (oxygen transport impedance) on the estimation of the intermediate and high frequency parameters (R_{hf}, R_{ct} and C_{dl}).

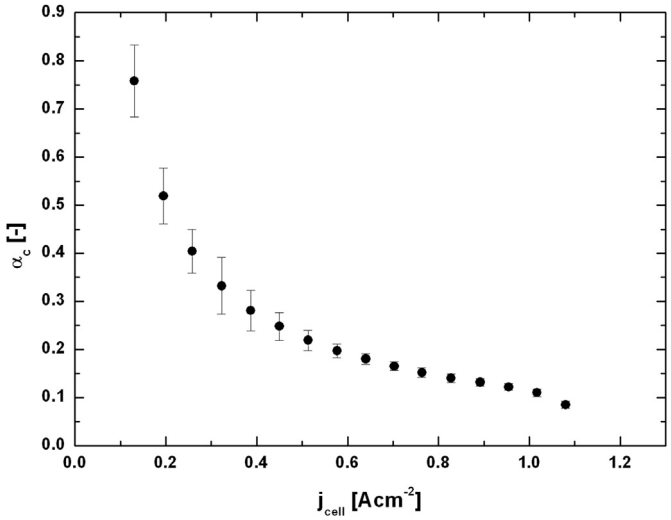

Fig. 7. Cathode charge transfer coefficient α_c deduced from EIS measurements vs. j_{cell}.

All sensitivity coefficients C_X are normalized according to

$$C_X = \frac{X}{||Z_{cell}||}\frac{dZ_{cell}}{dX}, \quad (20)$$

with $X = R_{hf}$, $R_{ct,c}$, $C_{dl,c}$, R_d, τ_d, $R_{ct,a}$, $C_{dl,a}$ and Z_{cell} standing for the global impedance of the MEA, as defined by Eq. (18). C_X is an indicator of the sensitivity of the cell impedance to the parameter X with absolute values varying between 0 and 1. It is generally considered that when the absolute value of C_X is lower than 0.05, the impact of X on the cell impedance is lower than the experimental data scattering. In this case, a consistent parameter estimation is not possible anymore.

The sensitivity coefficients C_X are complex functions of the model parameters. In what follows, the C_X are obtained using the impedance parameters that were estimated in the operating conditions given in section 3 at $j_{cell} = 0.5$ A cm^{-2} (Table 2).

4.2.1. Sensitivity analysis with reference to the cathode parameters

Fig. 8(a) and (b) show the real and imaginary parts of the sensitivity coefficients C_X relative to the cathode parameters as functions of the frequency ν in a range comprised between 1 mHz and 10 kHz. The absolute values of C_X may vary in other operating conditions. However, the curves in Fig. 8 reflect well the relative influence of the different model parameters over the whole fuel cell operating domain.

It can be seen that the sensitivity coefficients are significant in the frequency range 0.1 Hz − 1 kHz. For frequencies higher or lower than this interval, the values of C_X are either negligibly small ($C_X < 0.05$) or constant for several parameters indicating that correlations may exist between them. Measurements performed with frequencies beyond this interval would thus not contribute to a better precision. The observations relative to the sensitivity coefficients of the cathode parameters can be summarized as follows:

- The sensitivity coefficient of the high frequency resistance C_{Rhf} (black solid line in Fig. 8(a)) is a real number. R_{hf} is the parameter with the highest influence on the cell impedance for frequencies above 10 Hz: its sensitivity coefficient is higher than 0.4.
- The real and imaginary parts of the sensitivity coefficients relative to $R_{ct,c}$ (green dotted lines) and $C_{dl,c}$ (purple dashed lines) reach their maximum (absolute) values between 10 Hz and 1 kHz. In this range, $C_{Rct,c}$ and $C_{Cdl,c}$ climb to about 0.4.
- The sensitivities of the diffusion impedance parameters − C_{Rd} (pink dash-dot lines) and $C_{\tau d}$ (blue solid lines) − reach their highest values at frequencies below 10 Hz. These values are generally lower than those of the cathode reaction parameters: the maximum of C_{Rd} is about 0.3 and $C_{\tau d}$ does not exceed 0.1.

These results confirm that the time-scales of mass transport and of charge separation and transfer are clearly separated in this impedance model. R_{hf}, $R_{ct,c}$ and $C_{dl,c}$ can therefore be called *high frequency* parameters, whereas the parameters of the diffusion impedance (δ and R_d) are referred to as the *low frequency* parameters. These results also put forward that R_{hf}, $R_{ct,c}$ and $C_{dl,c}$ can be estimated without the use of an oxygen transport impedance when fitting the high frequency part of the spectra only. Note that this result is valid for the EEC in Fig. 2 only: sensitivity analyses are specific to each model and should be carried out systematically.

It has to be noted that the sensitivity coefficients relative to $R_{ct,c}$ and R_d show a similar behavior at intermediate frequencies indicating that these parameters could be correlated over this

Table 2
Mean cathode and anode impedance parameters with their corresponding standard deviations estimated from a series of 5 impedance spectra (Fig. 10) and anode parameters as they can be found in the literature 47 (third row).

R_{hf} [Ω cm^2]	$R_{ct,c}$ [Ω cm^2]	$C_{dl,c}$ [mF cm^{-2}]	R_d [Ω cm^2]	τ_d [s]	$R_{et,a}$ [Ω cm^2]	$C_{dl,a}$ [F cm^{-2}]	α [−]
0.156 ± 0.2%	0.27 ± 0.6%	22.4 ± 0.1%	–	–	–	–	–
0.153 ± 2%	0.23 ± 0.8%	19.7 ± 0.5%	0.158 ± 2%	0.066 ± 3%	–	–	–
0.148 ± 0.06%	0.23 ± 0.8%	19.7 ± 0.1%	0.157 ± 1%	0.066 ± 3%	0.005 ± 20%	0.2 ± 50%	1
–	–	–	–	–	0.007[a]	0.75[a]	0.97[a]

[a] Fit results obtained by Meland et al. [47] on a cell fed with hydrogen at both electrodes at $T = 50$ °C and $P = 1$ atm.

frequency range. It is thus possible that the choice of the oxygen transport model affects the estimation of the charge transfer resistance when using the Randles EEC. The impact of this possible correlation on the estimation of the high frequency parameters is treated with more details below.

4.2.2. Sensitivity analysis with reference to the anode parameters

For the sake of clarity, the anode sensitivity coefficients are plotted separately in Fig. 9 as functions of the frequency. Similarly to the cathode sensitivity parameters, $C_{Cdl,a}$ (red and pink solid lines) and $C_{Rct,a}$ (dark and light green dashed lines) reach their maximum (absolute) values at frequencies between 10 Hz and 1 kHz, but at slightly higher frequencies than the corresponding cathode sensitivities. However, the absolute values of the anode sensitivities do not exceed 0.01, whereas the cathode coefficients reach about 0.4. The sensitivity of the cell impedance relative to the cathode parameters is about 40 times higher than to those related to the anode. This leads to the conclusion that the anode can be neglected in the impedance model, which is consistent with results from previous articles [8,9,13,27,28]. It has to be noted that this conclusion is valid only when the anode operates normally (i.e. in the absence of phenomena such as fuel starvation, water flooding or electrode degradation).

As fuel cell impedance spectra are often depressed semicircles, Constant Phase Elements (CPE) are sometimes used to enhance the quality of the fitting curves [9,47–49]. There exist various expressions of the impedance of a constant phase element Z_{CPE} [48]. However, in most of the cases, Z_{CPE} is written as

$$Z_{CPE} = \frac{1}{C_{dl,a}(i\omega)^{\alpha}}, \tag{21}$$

where $\alpha \leq 1$. This impedance is purely resistive for $\alpha = 0$, capacitive for $\alpha = 1$ and inductive for $\alpha = -1$; generally $\alpha \in [0.5,1]$. The physical meaning of CPE is usually related to the distribution of the capacitance through the catalyst layer [9,50,51]. The impact of the CPE in the anode equivalent circuit is analyzed in Fig. 9: C_α (light and dark blue dash-dot lines) not only governs the anode impedance over the whole frequency range, but it has a similar behavior as $C_{Cdl,a}$, indicating a possible correlation between both parameters. A simultaneous estimation of the anode parameters is (most probably) not possible when using a CPE instead of a capacitance in this EEC. This could be confirmed experimentally: the fitting curves do not converge when using a CPE in the anode EEC: the exponent α (at least) has to be imposed as a fixed model parameter. In order to avoid problems related to the use of a CPE, a simple capacitance was used in the anode EEC.

4.2.3. Experimental validation of the numerical sensitivity analysis

The results of the (numerical) sensitivity analysis can be confirmed by fitting experimental spectra with the equivalent circuit of Fig. 2. Fig. 10 shows a mean EI spectrum (average values and standard deviations) resulting from a series of 5 spectra measured under identical conditions (those of the sensitivity analysis, cf. Section 3). For frequencies below 0.4 Hz, the data exhibit an important scattering which can be linked to the evacuation of water droplets through the air channel. Impedance

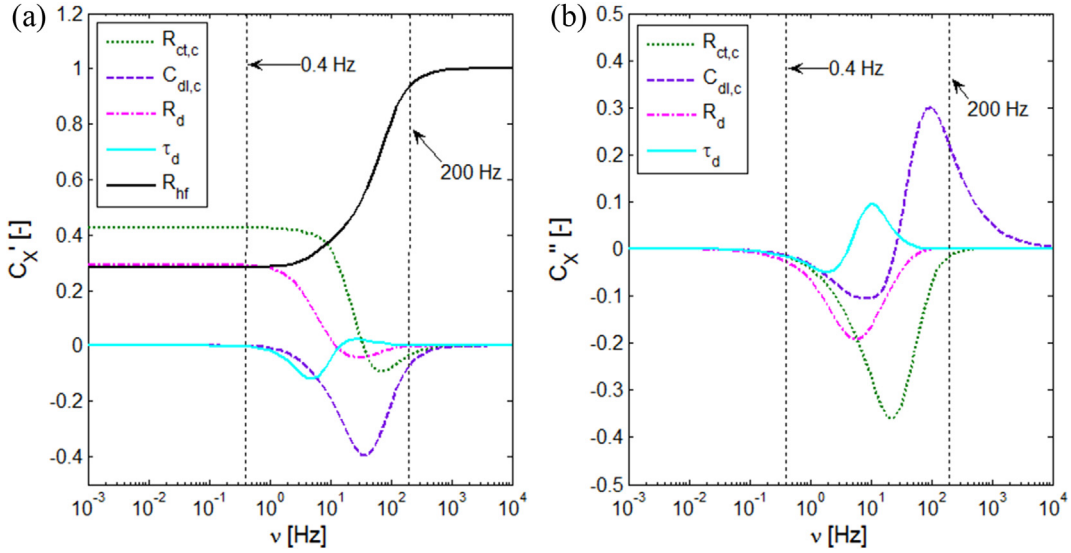

Fig. 8. Real (a) and imaginary part (b) of the cathode sensitivity coefficients C_X as functions of the frequency ν for the set of impedance parameters in Table 2; $X = R_{hf}$, $R_{ct,c}$, $C_{dl,c}$, R_d, τ_d, $R_{ct,a}$, $C_{dl,a}$.

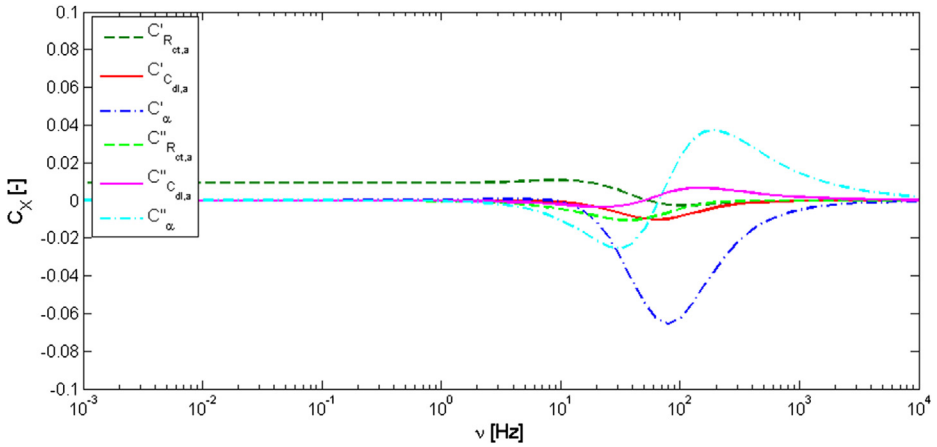

Fig. 9. Real and imaginary parts of the anode sensitivity coefficients as functions of the frequency using the set of impedance parameters in Table 2.

data measured at frequencies below 0.4 Hz are thus not retained for the parameter estimation. Furthermore, this avoids complications resulting from possible inductive features sometimes observed at low frequencies [8,36,52–54]. The experimental spectra exhibit also sometimes an inductive loop in the kHz regime, which is consistent with previous observations [9,54,55]. Our analyses show that the sensitivity coefficients reach significant values between 0.4 Hz and 200 Hz (Fig. 8) and that in addition, the model parameters do not seem to be correlated in this range. Consequently, parameter estimations are limited to this interval where inductive loops are without remarkable consequences. This allows also to exclude the straight line at 45° that appears in the kHz regime and which is linked to protonic resistance of the volumetric cathode [1,56,57].

Table 2 shows the estimated mean cathode and anode impedance parameters (leading to the theoretical impedance spectrum in Fig. 10; red curve) with their expected standard deviations. In the first row, we present the cathode parameters obtained using the Randles EEC only. They are consistent with values commonly found in the literature [27,58,59]. In addition, their corresponding standard deviations do not exceed 3%, which is an indicator of the validity of this parameters estimation.

The second row of Table 2 shows the parameters resulting from the estimation using the anode and cathode EEC (Fig. 2). Actually, the direct estimation of the 8 parameters is not possible because of cross-correlations between them. Therefore, the following method was employed:

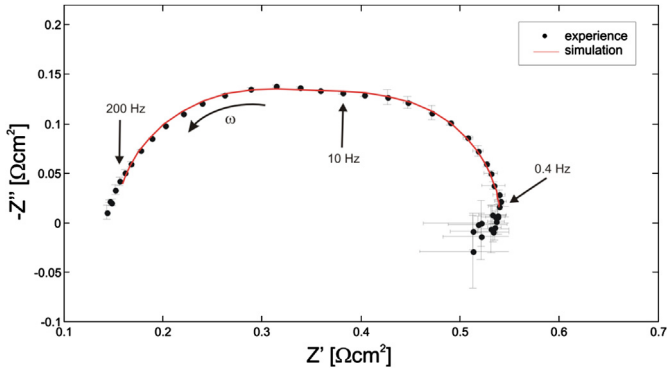

Fig. 10. Experimental mean spectrum resulting from a series of 5 measurements under identical conditions and theoretical spectrum computed after identification of the model parameters.

1. Estimation of the cathode parameters keeping constant the anode parameters.
2. Estimation of the anode parameters keeping constant the former estimated cathode parameters.
3. Re-estimation of the cathode parameters keeping constant again the anode parameters.

The values of the cathode parameters exhibit almost no variation between steps 1 and 3. It can thus be confirmed that the estimation of the anode parameters has no significant influence on the cathode parameters. Actually, the only difference lies in the value of R_{hf}: when considering the cathode only, R_{hf} corresponds to the sum of the high frequency resistance and the anode charge transfer resistance $R_{ct,a}$ resulting from the estimation when considering both electrodes.

Note that although our experimental values of $R_{ct,a}$ and $C_{dl,a}$ exhibit a scattering reaching 50%, they are in good agreement with those encountered in the literature for similar operating conditions [47] (third row of Table 2).

4.2.4. Correlations between the high and low frequency parameters

The results of the sensitivity analysis indicate a possible correlation between the high and low frequency parameters at intermediate frequencies. To clarify this point, the spectra in Fig. 10 were fitted with a simple EEC that accounts for charge separation and transport processes only (through R_{hf}, $C_{dl,c}$ and $R_{ct,c}$) which we refer to as the *RRC* equivalent circuit. The parameters obtained with the RRC and their corresponding standard deviations are given in Table 3. In order to facilitate the comparison with the parameters estimated with the full model including oxygen transport, Table 3 gives also the relative difference ΔX, defined as $|X_{RRC} - X_{Randles}|/X_{Randles}$, with $X = R_{hf}$, $R_{ct,c}$ and $C_{dl,c}$. If correlations exist at intermediate frequencies, the difference between the estimations obtained with the two EEC could be reduced by shifting the fit interval to higher frequencies. Therefore, the parameters estimations were carried out over three different frequency ranges: the maximum frequency is fixed at 200 Hz and the minimum frequency ν_{min} is set to 20 Hz, 50 Hz and 100 Hz. Indeed, ΔX decreases for the three parameters when ν_{min} is set to 50 Hz instead of 20 Hz. However, the following differences in the values and their variations can be observed for the three parameters:

- The high frequency resistance is only slightly affected by the change in the frequency range and ΔR_{hf} remains below 2% even when ν_{min} is set to 20 Hz. We can conclude that the high

Table 3
Mean cathode impedance parameters and standard deviations estimated from a series of 5 impedance spectra (Fig. 10) with a simple EEC consisting of R_{hf} in series with $R_{ct,c}$ and $C_{dl,c}$ in parallel. The table shows also the normalized difference in comparison to an estimation using the entire model including oxygen transport.

ν [Hz]	R_{hf} [Ω cm^2]	$R_{ct,c}$ [Ω cm^2]	$C_{dl,c}$ [mF cm^{-2}]	ΔR_{hf} [%]	$\Delta R_{ct,c}$ [%]	$\Delta C_{dl,c}$ [%]
20–200	0.156 ± 0.2%	0.269 ± 0.6%	22.4 ± 0.1%	1.8	17	14
50–200	0.151 ± 0.3%	0.239 ± 1%	19.9 ± 0.7%	1.3	3.9	0.7
100–200	0.148 ± 0.7%	0.207 ± 3.3%	18.5 ± 1.6%	3.2	9.9	6.3

frequency resistance can be considered as independent of the low frequency behavior of the spectra. This is consistent with the results of the sensitivity analysis showing that C_{Rhf} is not correlated with the other sensitivity coefficients.

- $\Delta C_{dl,c}$ and $\Delta R_{ct,c}$ depend strongly on the frequency range. The impact of ν_{min} is more important on $R_{ct,c}$ than on $C_{dl,c}$: $\Delta R_{ct,c}$ reaches 17% when ν_{min} is set to 20 Hz and about 4% when the parameters estimation starts at 50 Hz. In comparison, $\Delta C_{dl,c}$ decreases from 14% to 0.7% when ν_{min} is set to 50 Hz instead of 20 Hz. For an accurate estimation of $C_{dl,c}$ and $R_{ct,c}$ the use of an oxygen transport impedance is thus necessary.

Nevertheless, when starting the parameters estimation at frequencies above 50 Hz, ΔX remains below 4% for the three parameters, confirming that the simple RRC equivalent circuit is sufficient for the estimation of the high frequency impedance parameters in these conditions. It can be noted that when ν_{min} is further increased to 100 Hz, ΔX increases again: this is linked to the decrease of the amount of data available for the parameters estimation.

Finally, it should be mentioned that the results shown in this section are also validated by sensitivity analyses performed in other operating conditions (not presented here), starting from experimental data, as well as with series of 1000 numerically simulated and noised spectra.

5. Conclusions

In this work, we discussed the validity of the estimation of the high frequency impedance parameters characterizing the cathode of a H_2/air PEMFC, using the Randles EEC accounting for charge separation and transport processes through a high frequency resistance, a charge transfer resistance and a double-layer capacity. Oxygen transport is accounted for by a one-dimensional finite Warburg impedance. Since the mass transport limitations are negligible at the anode when the cell is fed with pure hydrogen, it is represented only by a charge transfer resistance in parallel with a capacitance.

The parameters characterizing the cathode reaction (the Tafel slope b, the charge transfer coefficient α_c and the exchange current density j_0) can be calculated starting from the charge transfer resistance. This allows us to estimate the electrode reaction parameters at a given operating point instead of giving only two (or three) averaged values being associated with the low (the intermediate) and the high current density regimes. Furthermore, the determination of b and α_c from the Tafel plot requires the measurement of a whole current–voltage curve and does not discriminate between losses due to mass transport and charge transfer. When using EIS the interpretation of one single impedance spectrum is sufficient for the determination of these parameters, which reduces drastically the measuring time.

Complementary sensitivity analyses were carried out in order to investigate the validity domain of the Randles EEC used for the estimation of the cathode parameters. The numerical results confirm that the cathode governs the cell impedance: the anode has no significant impact on the estimation of the cathode parameters and can be neglected. In addition, it is possible to determine the frequency range over which the cathode parameters have a significant impact on the cell impedance without being correlated to each other. Hence, we showed through the analysis of the sensitivity coefficients that R_{hf}, $C_{dl,c}$ and $R_{ct,c}$ influence the spectra rather in the high and intermediate frequency range, whereas the diffusion parameters of the Warburg impedance, R_d and τ_d, have a significant impact in the low frequency domain. However, the results of the sensitivity analysis put forward the existence of a correlation between the charge transfer resistance and the diffusion parameters at intermediate frequencies. These observations were also confirmed experimentally and the frequency range in which the high frequency parameters can be estimated independently of the diffusion impedance was determined.

Appendix A. Cathode charge transfer resistance at low current densities

In the sequel, the derivation of the cathode charge transfer resistance at low current densities is presented. To start, the oxygen reduction reaction of the form $1/2O_2 + 2H^+ + 2e^- \rightarrow H_2O$ is described in a general way by the Butler–Volmer equation according to

$$j_{f,c} = j_0 \left[\frac{c_{H_2O}(0)}{c^*_{H_2O}} \exp\left(\frac{\alpha_c 2F}{RT}\eta_c\right) - \frac{c_{O_2}(0)}{c^*_{O_2}} \exp\left(\frac{-(1-\alpha_c)2F}{RT}\eta_c\right) \right] \tag{A.1}$$

where $c_k(x=0)$ $(k = H_2O,O_2)$ stands for the agent concentrations at the reaction interface at $x = 0$ and c^*_k for their bulk concentrations. For very low current densities (low overpotentials), the exponential can be approached by $\exp x = 1 + x$. In addition, mass transfer limitation are negligible and the species concentrations at the reaction sites can be considered identical to their bulk values $c_k(0) = c^*_k$. The above equation reduces consequently to

$$j_{f,c} = j_0 \left(\frac{\alpha_c 2F}{RT}\eta_c - \frac{-(1-\alpha_c)2F}{RT}\eta_c \right) = \frac{2Fj_0}{RT}\eta_c. \tag{A.2}$$

Combination of (A.2) with the definition of the charge transfer resistance at the cathode (12) results then in

$$R_{ct} = \frac{RT}{2Fj_0}, \tag{A.3}$$

showing that R_{ct} is independent from the charge transfer coefficient in this current regime. This is a general result for RedOx reactions in electrochemical systems. Note however that the number of exchanged electrons might change depending on the reaction mechanism.

Nomenclature

A_{macro}	[cm^2] MEA flat surface
A_{Pt}	[cm^2] catalytic active area
b [V]	Tafel slope
b_{10}	[V dec^{-1}] Tafel slope
C_{dl}	[F cm^{-2}] double-layer capacity
c_i	[mol cm^{-3}] concentration of species i
c^*_i	[mol cm^{-3}] equilibrium concentration of species i
D^{eff}	[m^2 s^{-1}] effective diffusion coefficient

E_0 [V] open circuit voltage (OCV)
E_{cell} [V] cell voltage
F [C mol^{-1}] Faraday's constant, $F = 96485$
j_{cell} [A cm^{-2}] cell current density
j_0 [A cm^{-2}] exchange current density
j_c [A cm^{-2}] capacitive current density
j_f [A cm^{-2}] faradaic current density
P [Pa] gas pressure
R [J mol^{-1} K^{-1}] gas constant, $R = 8.314$
R_{ct} [Ω cm^2] charge transfer resistance
R_d [Ω cm^2] diffusion resistance
R_{hf} [Ω cm^2] high frequency resistance
S_i [−] stoichiometric factor of species i
T [K] temperature
Z [Ω cm^2] impedance

Greek letters

α [−] CPE parameter
α_k [−] charge transfer coefficient at electrode k
γ [−] electrode roughness
δ [μm] diffusion medium thickness
ϵ [−] porosity
η_k [V] activation overpotential at electrode k
ν [Hz] frequency
τ_d [s] characteristic diffusion time
ω [rad s^{-1}] angular frequency

Sub-/superscripts

a anode
c cathode
c_{O_2} oxygen concentration
W Warburg

References

[1] T. Springer, T. Zawodzinski, M. Wilson, S. Gottesfeld, J. Electrochem. Soc. 143 (1996) 587–599.
[2] V. Paganin, C. Oliveira, E. Ticianelli, T. Springer, E. Gonzalez, Electrochim. Acta 43 (1998) 3761–3766.
[3] T. Okada, G. Xie, Y. Tanabe, J. Electroanal. Chem. 413 (1996) 49–65.
[4] X. Yuan, H. Wang, J. Colin Sun, J. Zhang, Int. J. Hydrogen Energy 32 (2007) 4365–4380.
[5] S.M.R. Niya, M. Hoorfar, J. Power Sources 240 (2013) 281–293.
[6] T. Springer, I. Raistrick, J. Electrochem. Soc. 136 (1989) 1594–1603.
[7] I. Raistrick, Electrochim. Acta 35 (1990) 1579–1586.
[8] O. Antoine, Y. Bultel, R. Durand, J. Electroanal. Chem. 499 (2001) 85–94.
[9] M. Ciureanu, R. Roberge, J. Phys. Chem. B 105 (2001) 3531–3539.
[10] N. Wagner, J. Appl. Electrochem. 32 (2002) 859–863.
[11] S. Lee, S. Mukerjee, J. McBreen, Y. Rho, Y. Kho, T. Lee, Electrochim. Acta 43 (1998) 3693–3701.
[12] Q. Guo, M. Cayetano, Y.-M. Tsou, E. De Castro, R. White, J. Electrochem. Soc. 150 (2003) A1440–A1449.
[13] N. Fouquet, C. Doulet, C. Nouillant, G. Dauphin Tanguy, B. Ould Bouamama, J. Power Sources 159 (2006) 905–913.
[14] J.-M. Le Canut, R. Abouatallah, D. Harrington, J. Electrochem. Soc. 153 (2006) A857–A864.
[15] A. Lamibrac, G. Maranzana, O. Lottin, J. Dillet, J. Mainka, S. Didierjean, A. Thomas, C. Moyne, J. Power Sources 196 (2011) 9451–9458.
[16] N. Wagner, M. Schulze, Electrochim. Acta 48 (2003) 3899–3907.
[17] M. Kumagai, S.-T. Myung, T. Ichikawa, H. Yashiro, J. Power Sources 195 (2010) 5501–5507.
[18] J. Randles, Discuss. Faraday Soc. 1 (1947) 11.
[19] E. Warburg, Ann. Phys. Chem. 69 (1899) 493–499.
[20] J. Mainka, G. Maranzana, J. Dillet, S. Didierjean, O. Lottin, J. Electrochem. Soc. 157 (2010) B1561–B1568.
[21] J. Mainka, Local Impedance in H_2/air Proton Exchange Membrane Fuel Cells (PEMFC) - Theoretical and Experimental Investigations, Ph.D. thesis, Univeristé Henri Poincaré - INPL-LEMTA, Nancy, 2011, http://perso.ensem.inpl-nancy.fr/Olivier.Lottin/FicEssai/TheseMainka.pdf.
[22] J. Mainka, G. Maranzana, A. Thomas, J. Dillet, S. Didierjean, O. Lottin, Fuel Cells 12 (2012) 848–861.
[23] Arvind Parthasarathy, Bhasker Dave, Supramaniam Srinivasan, A. John Appleby, Charles R. Martin, J. Electrochem. Soc. 139 (1992) 1634–1641.
[24] M. Boillot, Validation expérimentale d'outils de modélisation d'une pile à combustible de type PEM, Ph.D. thesis, INPL-ENSIC, Nancy, 2005.
[25] A. Parthasarathy, S. Srinivasan, A. Appleby, C.R. Martin, J. Electrochem. Soc. 139 (1992) 2530–2537.
[26] V. Danilov, M. Tade, Chem. Eng. J. 156 (2010) 496–499.
[27] M. Rubio, A. Urquia, R. Kuhn, S. Dormido, J. Power Sources 183 (2008) 118–125.
[28] J. Deseure, J. Power Sources 178 (2008) 323–333.
[29] I. Schneider, S. Freunberger, D. Kramer, A. Wokaun, G. Scherer, J. Electrochem. Soc. 154 (2007a) B383–B388.
[30] I. Schneider, D. Kramer, A. Wokaun, G. Scherer, J. Electrochem. Soc. 154 (2007b) B770–B782.
[31] G. Maranzana, J. Mainka, O. Lottin, J. Dillet, A. Lamibrac, A. Thomas, S. Didierjean, Electrochim. Acta 83 (2012) 13–27.
[32] W. Sun, B. Peppley, K. Karan, Electrochim. Acta 50 (2005) 3359–3374.
[33] J. Bockris, A. Reddy, Modern Electrochemistry, Plenum Publishing Corporation, 1973.
[34] B. Conway, B. Tilak, Electrochim. Acta 47 (2002) 3571–3594.
[35] H. Wendt, E. Spinacé, A. Oliveira Neto, M. Linardi, Quim. Nova 28 (2005) 1066–1075.
[36] M. Ciureanu, H. Wang, J. Electrochem. Soc. 146 (1999) 4031–4040.
[37] J. Mainka, G. Maranzana, J. Dillet, S. Didierjean, O. Lottin, in: D. Stolten, T. Grube (Eds.), 18th World Hydrogen Energy Conference 2010-WHEC 2010: Parallel Sessions Book 1: Fuel Cell Basics/Fuel Infrastructures, Schriften des Forschungszentrums Jülich/Energy & Environment, Forschungszentrum Jülich GmbH, Zentralbibliothek, Verlag, Essen (Germany), 2010, pp. 37–44. ISBN: 978-3-89336-651-4, ISSN: 1866-1793.
[38] S. Torquato, Random Heterogeneous Materials: Microstructure and Macroscopic Properties, Springer, 2002. ISBN 13: 978-0387951676.
[39] G. Archie, Trans. AIME 146 (1942) 54–61.
[40] A. Thomas, G. Maranzana, S. Didierjean, O. Lottin, J. Dillet, A. Lamibrac, in: Proceedings of the Fundamentals and Developments of Fuel Cells Conference 2011, 19th-21st January 2011, Grenoble, France, 2011. ISBN: 978-2-7566-2970-7.
[41] J. Lagarias, J. Reeds, M. Wright, P. Wright, SIAM J. Optimizat. 9 (1999) 112–147.
[42] F. Gloaguen, R. Durand, J. Appl. Electrochem. 27 (1997) 1029–1035.
[43] O. Antoine, Y. Bultel, R. Durand, P. Ozil, Electrochim. Acta 43 (1998) 3681–3691.
[44] A. Parthasarathy, C.R. Martin, S. Srinivasan, J. Electrochem. Soc. 138 (1991) 916–921.
[45] W. Sun, B. Peppley, K. Karan, J. Power Sources 144 (2005) 42–53.
[46] S. Chupin, T. Colinart, S. Didierjean, Y. Dubé, K. Agbossou, G. Maranzana, O. Lottin, J. Power Sources 195 (2010) 5213–5227.
[47] A.-K. Meland, S. Kjelstrup, D. Bedeaux, J. Memb. Sci. 282 (2006) 96–108.
[48] J.-B. Jorcin, M. Orazem, N. Pébère, B. Tribollet, Electrochim. Acta 51 (2006) 1473–1479.
[49] S. Roy, M. Orazem, J. Electrochem. Soc. 156 (2009) B203–B209.
[50] C. Hitz, A. Lasia, J. Electroanal. Chem. 500 (2001) 213–222.
[51] C.-H. Kim, S.-I. Pyun, J.-H. Kim, Electrochim. Acta 48 (2003) 3455–3463.
[52] I. Schneider, M. Bayer, A. Wokaun, G. Scherer, J. Electrochem. Soc. 155 (2008) B783–B792.
[53] M. Mathias, D. Baker, J. Zhang, Y. Liu, W. Gu, in: ECS Transactions, vol. 13, 2008, pp. 129–152.
[54] S. Roy, M. Orazem, in: ECS Transactions, vol. 13, 2008, pp. 153–169.
[55] J.P. Diard, B. Le Gorrec, C. Montella, C. Poinsignon, G. Vitter, J. Power Sources 74 (1998) 244–245.
[56] M. Eikerling, A. Kornyshev, J. Electroanal. Chem. 475 (1999) 107–123.
[57] Y. Bultel, L. Genies, O. Antoine, P. Ozil, R. Durand, J. Electroanal. Chem. 527 (2002) 143–155.
[58] S. Rodat, S. Sailler, F. Druart, P.-X. Thivel, Y. Bultel, P. Ozil, J. Appl. Electrochem. 40 (2010) 911–920.
[59] R. Makharia, M. Mathias, D. Baker, J. Electrochem. Soc. 152 (2005) A970–A977.